Nuclear Materials and Energy 31 (2022) 101172

Contents lists available at ScienceDirect

Nuclear Materials and Energy

journal homepage: www.elsevier.com/locate/nme

Influence of 2 (wt%) titanium addition on the oxidation resistance of tungsten

P. Pérez [a], M.A. Monge [b,*]

[a] Centro Nacional de Investigaciones Metalúrgicas, Departamento de Metalurgia Física, CENIM-CSIC, Avda. Gregorio del Amo 8, 28040 Madrid, Spain
[b] Universidad Carlos III de Madrid, Departamento de Física, Avda. de la Universidad 30, 28911 Leganés, Madrid, Spain

ARTICLE INFO

Keywords:
Tungsten
Tungsten oxide
Titanium alloying
High-temperature oxidation

ABSTRACT

The oxidation behaviour of W-2Ti (wt%) alloy has been evaluated in dry air at 600, 700 and 800 °C for 100 h and the kinetics compared with those for pure tungsten. Titanium addition exerts a beneficial effect on the oxidation resistance of pure tungsten. The mass gain is almost five times smaller than in the case of commercial tungsten and three times smaller than that of tungsten prepared by powder metallurgy at 600 °C. This effect is even higher at 700 and 800 °C, where the titanium addition suppresses catastrophic oxidation of pure tungsten. Major influence of titanium regards the suppression of massive microcracking in the scale, avoiding the development of the typical non-protective multilayered scale pattern formed on pure tungsten.

1. Introduction

Tungsten is considered the best candidate material for some of the fusion engineering most demanding applications such as the armour of the divertor, the first wall components and the structural components of the blanket, due to its unique combination of properties [1,2]. Tungsten has a very high melting temperature and thermal conductivity, and also exhibits a good sputtering and radiation resistance to the 14 MeV fusion neutrons [3,4]. Furthermore, it is one of the few elements with low activation under irradiation with the 14 MeV fusion neutron [5]. One of the last modifications of the ITER (International Thermonuclear Experimental Reactor) design before its construction started was the introduction of W monoblocks in the vertical target of the divertor to assess this material in a truly representative service environment [6].

Even though the results of the extensive qualification program developed by the ITER Organization (IO) support its suitability as material for the plasma facing components, some challenges remain not only concerning the performance of W in more advanced fusion reactors under design, such as DEMO, but also with the safety hazards of the use of tungsten under some accident scenarios of a fusion reactor due to its low oxidation resistance [7,8].

A loss of the vacuum integrity of the vessel (LOVA) would produce the full oxidation of the W components, the formation of highly volatile radioactive tungsten oxides and the possible emission of this waste to the environment [9]. A much worse accident would be a LOVA in conjunction with a LOCA accident (Lost of Coolant Accident) or malfunction of the first wall cooling systems, that would produce the rise of the temperature of the first wall components up to ~1200 °C, maintaining the temperature over ~500 °C for a period longer than ten days due to the nuclear decay heat, with estimated sublimation rates of the W oxides for a full W armoured reactor of 10–100 kg h^{-1} [9]. Moreover, in the next generation of fusion reactors neutron fluxes will be higher than in ITER, resulting in significantly higher tungsten transmutation rates and the accumulation of Re, Ta and Os, which are the primary transmutation products for W. These would worsen the consequences of a LOVA accident due to the formation of highly toxic and volatile osmium oxides [10].

This research is the continuation of a series of published works devoted to the study of the temperature oxidation behaviour of pure tungsten, tungsten alloyed with low activation refractory elements (Ta and V) and tungsten reinforced with different dispersions of hard particles (Y_2O_3 and TiC) [8,11,12,13]. The results show that W with a small addition of Ti exhibits the best oxidation resistance of all studied materials, significantly increasing the oxidation resistance with the temperature. The work focuses on the study of tungsten with 2 %wt. Ti because previous results have shown that a higher Ti content produced an alloy with a less refined microstructure and slightly lower mechanical properties, see results in Refs. [14–16].

* Corresponding author.
E-mail address: mmonge@fis.uc3m.es (M.A. Monge).

https://doi.org/10.1016/j.nme.2022.101172
Received 29 November 2021; Received in revised form 16 March 2022; Accepted 19 March 2022
Available online 21 March 2022

2. Experimental procedure

W-2wt%Ti alloy (hereinafter W-2Ti) was prepared from tungsten and titanium elemental powders from Alfa Aesar© (Thermo Fisher (Kandel) GmbH, Germany), with purities of 99.94% and 99.97%, respectively. The particle sizes of the elemental powders were in the range 1–5 μm for tungsten, and smaller than 100 μm for titanium. The processing of the material was performed under a high purity argon atmosphere following a powder metallurgy route consisting of mechanical alloying in a high-energy planetary ball mill for 75 h and subsequent consolidation by HIP for 2 h at 1300 °C and 195 MPa. A detailed description of the production route can be found elsewhere. Two materials have been used as reference: a billet of pure W (PM-W) prepared following the W-2Ti production route and commercial tungsten (CP-W) in compliance with the ITER requirements for tungsten in divertor applications based on ASTM B760 specification.

Fig. 1 shows the microstructure of the W-2Ti alloy in the as-HIP condition. The HIP treatment appears to produce some titanium segregation giving rise to the formation of small titanium pools. The W-2Ti alloy exhibit an intermingled grain structure that consists of a population of submicron-sized grains and another one of coarser grains with sizes around 1 μm. EDX (Energy Dispersive X-Ray Analysis) analysis confirms that the alloy consists in tungsten with titanium in solid solution, being the titanium pools only composed of this element within the sensitivity of this technique. The microstructure and mechanical properties have been reported elsewhere [15].

Oxidation tests were carried out on coupons 10 × 10 × 1 mm^3. All major surfaces were abraded on successively finer silicon carbide papers, then mechanically polished with 1 μm diamond paste and cleaned with ethanol. Mass gain curves in the temperature range from 600 °C to 800 °C were determined by continuous isothermal thermogravimetry for exposures up to 100 h using a CI PRECISION MK2-M5 microbalance. Samples were suspended inside a quartz glassware system and inserted in a vertical tube furnace. Oxidation tests were carried out under a continuous flow of 50 ml/min of dry air (dewpoint below −40 °C) supplied by an electric compressor [8,11,12,13]. The oxidation kinetics were determined by adjusting the mass gain curves to a power law of the form $\Delta W = kt^n$ (ΔW is the mass gain per unit area, k the oxidation rate constant, n the rate exponent, and t the exposure time).

The characterization of the oxide scale was done on samples used for mass-gain determination, as well as on samples isothermally oxidized for different exposure times. Cross-sections were prepared by conventional metallographic techniques. To prevent scale loss during the metallographic preparation of the samples, the surfaces were coated first with a thin sputtered gold layer and then with a thicker layer of electrolytically deposited copper. Surfaces and cross-sections of the oxidized specimens were studied by scanning electron microscopy (SEM). Phase identification of the oxide scale was performed by X-ray diffraction (XRD) using Co-K_α radiation and energy dispersive X-ray microanalysis (EDX).

3. Results

Mass gain curves of the W-2Ti alloy oxidized in dry air at 600, 700 and 800 °C are presented in Fig. 2, yielding mass gain values of 2, 13 and 81 mg/cm^2 after 100 h of exposure at 600, 700 and 800 °C, respectively. At 600 and 700 °C, oxidation process proceeds uniform over the entire exposure time at which the kinetics follow quasi-parabolic laws ($n \approx 0.75$) and almost parabolic laws (n = 0.6), respectively. This indicates that the oxide scale established at 700 °C is more protective than that formed at 600 °C. At 800 °C, the oxidation behaviour is more complex than that found at 600 and 700 °C because the curve alternates periods at which the oxidation rate slows down to minimum values, with periods at which the oxidation rate is significantly accelerated (see periods of time identified with arrows in Fig. 2). At short oxidation times, the thermogravimetric curve shows a uniform mass gain from the initial stages of oxidation with a mass gain of 33.4 mg/cm^2 in the first 40 h of exposure. During this initial stage, the kinetics are governed by parabolic laws as the oxidation exponent is 0.5. Mass gain is progressively accelerated in the following 20 h, with a mass gain in this period of 20.6 mg/cm^2. The oxidation exponent reaches a value of 1.6 during this stage of oxidation, so the kinetics are governed by laws higher than linear. This behaviour is repeated during further exposure, although the time for the occurrence of slow and rapid oxidation periods tends to shorten as the oxidation proceeds.

The colour of the oxide scale after exposure for 100 h at 600 and 700 °C is grey, but at 800 °C it has the typical yellowish colour of the scale generated on pure tungsten with short wings at the edges [8].

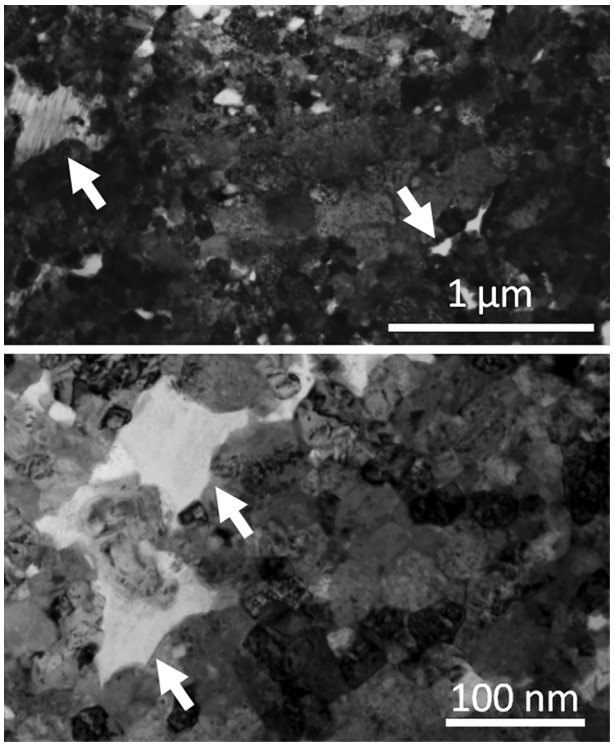

Fig. 1. Bright-field transmission electron microscopy images (TEM) showing the equiaxed microstructure of W-2Ti alloy. Some segregation of titanium is observed forming titanium pools (white arrows). The samples were prepared by focused ion beam (FIB) with Ga^+ ions close to normal incidence.

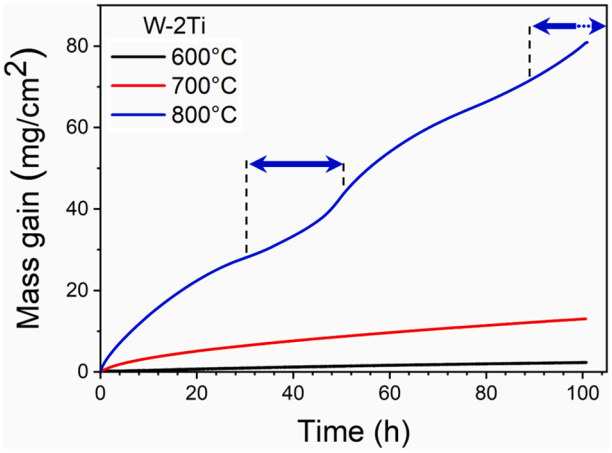

Fig. 2. Isothermal mass gain curves for W-2Ti oxidized for 100 h at 600, 700 and 800 °C in dry air. The horizontal arrows mark the periods at which the oxidation rate is accelerated at the testing temperature of 800 °C.

According to the XRD pattern of Fig. 3, the scale consists exclusively of the monoclinic WO_3 oxide, not appearing reflections of Ti-rich or mixed W-Ti oxides, probably due to the lower volume fraction of Ti-containing phases in the alloy. Since pure WO_3 colour is yellow, the change in colour of the oxide could be attributed to the dissolution of some titanium in the crystalline structure of WO_3 [17]. It is worth noting that information provided by XRD measurements is restricted to the outermost part of the scale due to the high average atomic number of tungsten oxides. Thus, changes in the composition of the oxides composing the scale cannot be ruled out in the samples subject to high mass gains, i.e. the samples oxidized at 700 and 800 °C.

Surface views of the sample oxidized at 600 °C evidence extensive cracking which appears as an irregular mesh, although the scale remains adhered to the metallic substrate (see Fig. 4). Since there is not a change in the oxidation rate once the steady state is achieved, formation of these cracks are surely the result of large strains induced in the scale by thermal stresses and/or the considerable changes in volume associated with allotropic transformations of tungsten oxides during cooling, especially WO_3 [18]. Minor cracks are clearly visible in Fig. 4a as grey or dark regions with a linear crack in the middle. In addition, other still minor cracks are randomly distributed on the surface of the scale associated with the development of small protuberances. A close magnification of the scale, Fig. 4b, reveals a smooth dark scale overgrown by small crystals, not larger than 0.5 μm. Similarly, the surface of the oxide scale after 100 h at 700 °C presents a continuous uniform oxide scale spattered by numerous protuberances cracked at the top (Fig. 5). A detail observation of the uniform scale reveals a continuous fine-grained scale with a crystal size around 150–200 nm which is overgrown by coarse-grained clusters (crystal size up to 600 nm). The amount of coarse oxide crystals overgrowing the smooth oxide layer is much higher at 700 °C, as can be observed by comparing Fig. 4 and the inset of Fig. 5a, along with a noticeable increase in the size of the nodules. These nodules are usually divided by several cracks running from the base of the nodule towards its top, where the size of oxide crystals achieves the maximum values, from 1 to 2 μm, as observed in Fig. 5b. At this temperature, parts of the scale spall off during cooling, leaving a thin fine-grained oxide layer close to the metal substrate. The aspect of the surface of the sample oxidized at 800 °C for 30 min resembles rather well that of the sample oxidized at 600 °C for 100 h (Fig. 6a). This similitude in the surface morphology among both scales would indicate that oxidation proceeds in the same way during the initial stages of oxidation at 800 °C and after 100 h of exposure at 600 °C, as it could be expected from their similar mass gain values (1.05 mg/cm^2 after 30 min of exposure at 800 °C against 2.3 mg/cm^2 for the sample exposed 100 h at 600).

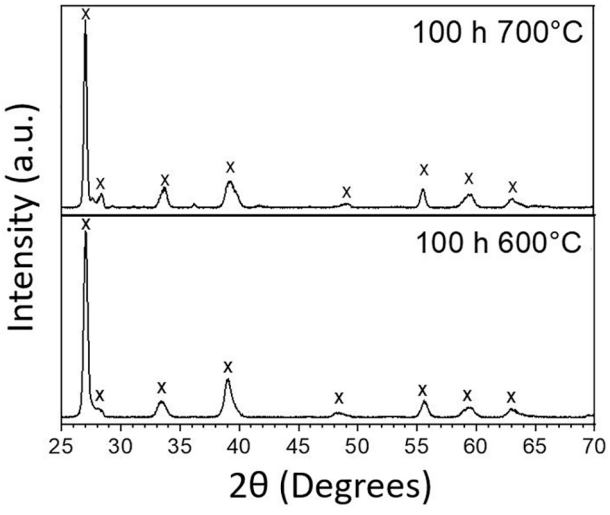

Fig. 3. XRD pattern of the oxide scale formed on W-2Ti alloy after oxidation at 600 °C for 100 h (×WO_3).

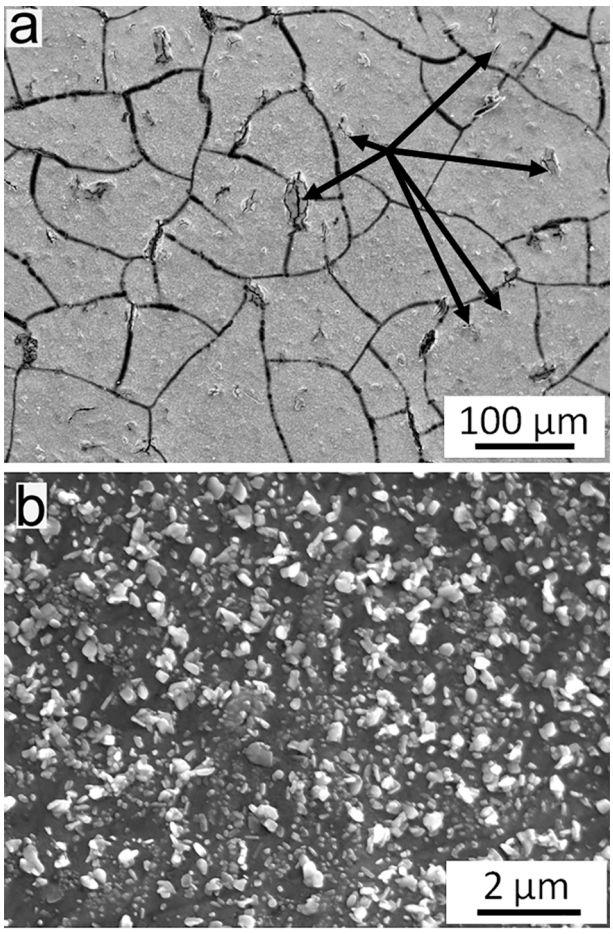

Fig. 4. Surface views of the scale formed over the W-2Ti alloy after oxidation at 600 °C for 100 h in dry air. (a) General view of the scale showing macro- and microcracking. Black arrows marked some examples of the microcracks present in the scale. (b) Close magnification of the surface scale showing the morphology of oxide crystals.

However, the morphology of the scale evolves more rapidly to that observed after 100 h of exposure at 700 °C as the oxidation test progresses (Fig. 6b). Thus, the smooth scale is almost totally overgrown by coarse oxide crystals after 30 h of exposure at 800 °C (see the inset of Fig. 6b). This morphology hardly changes for longer exposure times, as Fig. 6c shows for the sample oxidized 100 h. Compared to the sample exposed 30 h, only a complete densification of the outermost layer consisting of coarse crystal oxides is noticed. As already observed at lower temperatures, the oxide scales readily cracks and spalls off during cooling irrespective the exposure time.

Fig. 7a depicts a cross-section of the oxide scale of W-2Ti exposure at 600 °C, showing that the thickness of the scale formed after 100 h is about 20 μm. The scale is very uniform and homogeneous in thickness and it clearly matches the underlying microstructure of the alloy, so the isolated black regions embedded inside the oxide scale resemble fairly well the Ti-rich pools embedded in the tungsten matrix (see the inset of Fig. 7a). Perpendicular cracks, with a characteristic separation of ≈100–200 μm between them, run across the entire thickness of the scale. These cracks correspond to those observed in surface views of Fig. 4a. No evidence of cracks running parallel to the metal surface, as usually reported during oxidation of pure tungsten [8], is found within the scale. The nature of the scale developed at 700 °C is similar to that found after oxidation at 600 °C, but the thickness is kept uniform at about 105 μm, as can be checked in Fig. 7b. A close view of the scale allows to distinguishing some differences between the upper and lower halves of the scale; the outer half of the scale, about 65 μm in thickness, is less

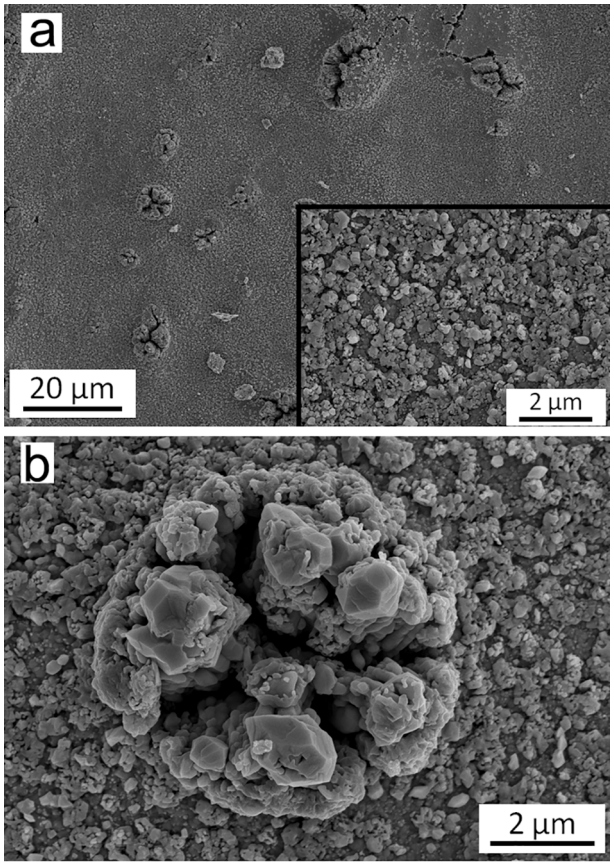

Fig. 5. (a) Surface view of the scale formed over the W-2Ti alloy after oxidation at 700 °C for 100 h in dry air. The morphology of tungsten oxide crystals is shown in the inset. (b) A typical example of the nodules developed on the surface of the scale.

compact than the 40 µm thick innermost half which presents a much finer microstructure (see inset of Fig. 7b).

At 800 °C, cross sections reveal significant differences in the structure of the scale with the exposure time. A relatively dense scale of about 2.5–3 µm is formed after 30 min of oxidation (Fig. 8). The isolated porosity observed in the scale coincides with the titanium pools of the alloy, which are embedded by the scale as it grows inwards into the metallic substrate. This layer considerably thickens as the oxidation progresses, and after 30 h of oxidation the thickness of the oxide scale is close to 400 µm (Fig. 9). In the central part of the scale a thick discontinuity is generated, dividing the scale in almost two halves, the outer part of the scale is 220 µm thick while the inner part is about 140 µm. At both sides, the structure of the scale resembles that found for the sample oxidized at 700 °C, although the innermost part of the scale exhibits large isolated cavities randomly distributed across its thickness.

A similar structure of the scale is observed in the sample oxidized for 100 h, but in this case two discontinuities are seen, so the scale could be considered to be subdivided into three layers with identical visual appearance, which are separated from each other by an almost continuous cavity/crack, as can be observed in Fig. 10. The total thickness of the scale is around 810 µm; where the first 230 µm corresponds to the outermost part of the scale from the surface to the first discontinuity, the following 340 µm to central part of the scale comprised between the two discontinuities and the last 240 µm to the innermost part of the scale from the second discontinuity to the metallic substrate. As observed at 700 °C, there is a gradient in the amount of small cavities present along the thickness of the scale that increases towards the metallic substrate.

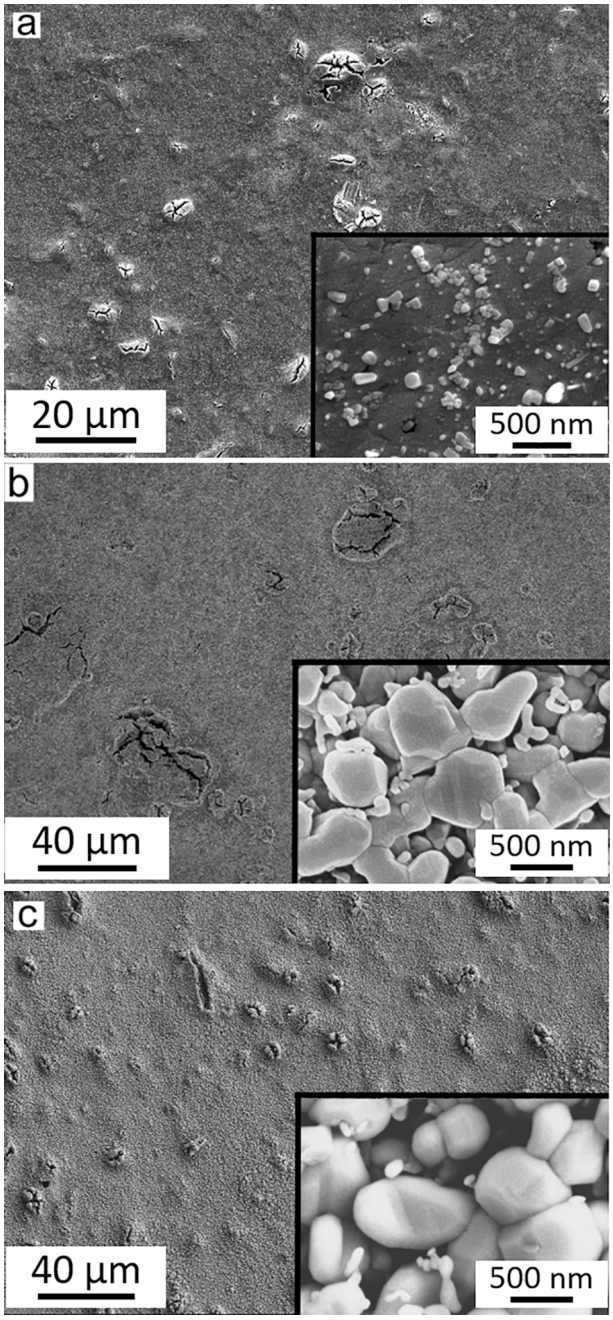

Fig. 6. Surface views of the scale formed over the W-2Ti alloy after oxidation in dry air at 800 °C for several times: (a) 30 min, (b) 30 h and (c) 100 h. The morphology of the scale is shown in the corresponding insets.

4. Discussion

The temperature of 600 °C is considered the maximum temperature at which the oxide scale developed on pure tungsten can provide some protectiveness in air [12,19,20]. Above this temperature, linear oxidation kinetics as well as WO_3 volatilization precludes the use of pure tungsten at high temperatures in oxidising atmospheres. The beneficial effect of 2 wt% Ti addition on the oxidation resistance of tungsten at 600 °C is clearly observed in the thermogravimetric curves of Fig. 11, that compares the mass gain curves of the W-2Ti alloy with those obtained for CP-W and PM-W. This result confirms the beneficial effect of titanium additions reported during short-term oxidation resistance, up to 30 min, for W-Ti coatings between 600 and 1000 °C [21,22], although the titanium content in the coating was much higher (10 wt%).

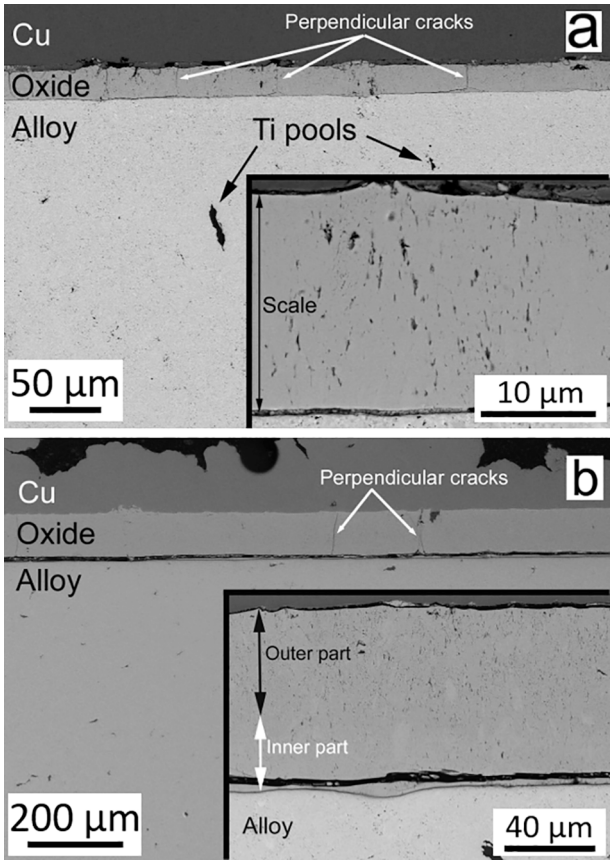

Fig. 7. Cross section of the scale formed on the W-2Ti alloy at different temperatures: a) After 100 h of exposure at 600 °C, b) After 100 h of exposure at 700 °C. Close views of the scales are presented in the corresponding insets.

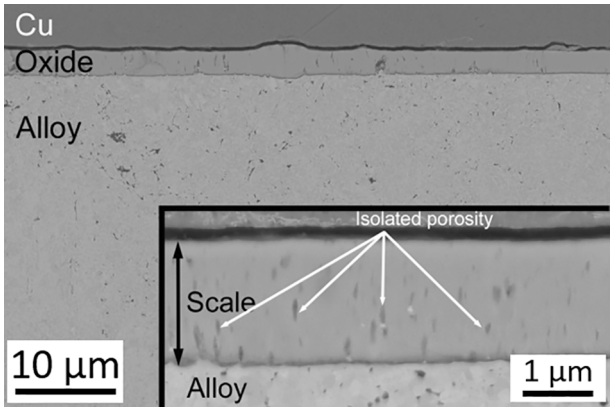

Fig. 8. Cross section of the scale formed on the W-2Ti alloy after 30 min of exposure at 800 °C. The inset shows a close view of the scale.

At 600 °C, titanium addition induces a significant decrease in the mass gain, being its value about a half and one-fourth of the corresponding values reported for PM-W and CP-W, respectively [8,12]. Curiously, the mass gain reduction cannot be directly associated itself with the formation of a more protective oxide. The main oxide constituting the scale is monoclinic WO_3 which is the same oxide reported in previous studies for pure tungsten [8]. Furthermore, the yellowish colour characteristic of WO_3 changes to the grey colour of the oxide formed over the W-2Ti alloy not only at 600 °C but also after exposure at 700 °C, and finally the colour turns yellow after exposure at 800°. Although the oxide is the same, WO_3 according to XRD pattern of Fig. 3,

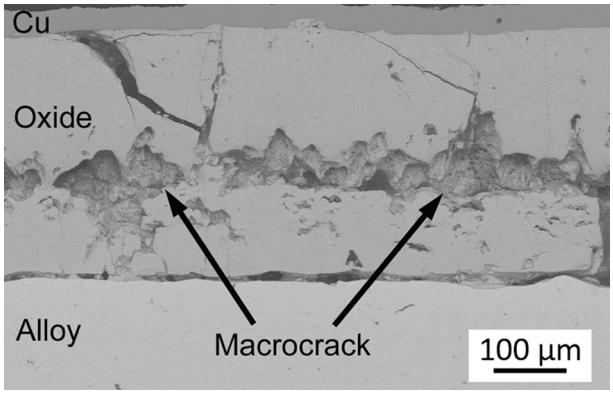

Fig. 9. Cross section of the scale formed on the W-2Ti alloy after 30 h of exposure at 800 °C.

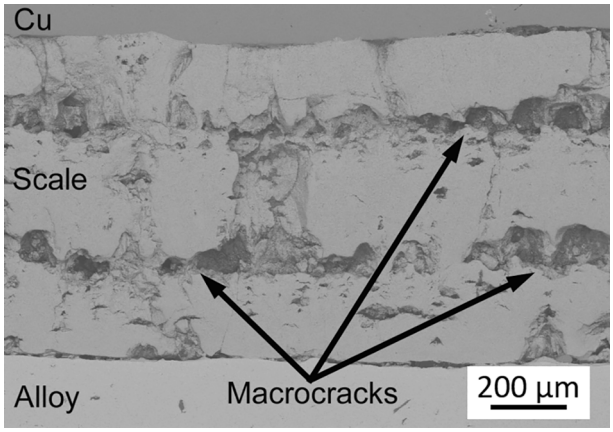

Fig. 10. Cross section of the scale formed on the W-2Ti alloy after 100 h of exposure at 800 °C.

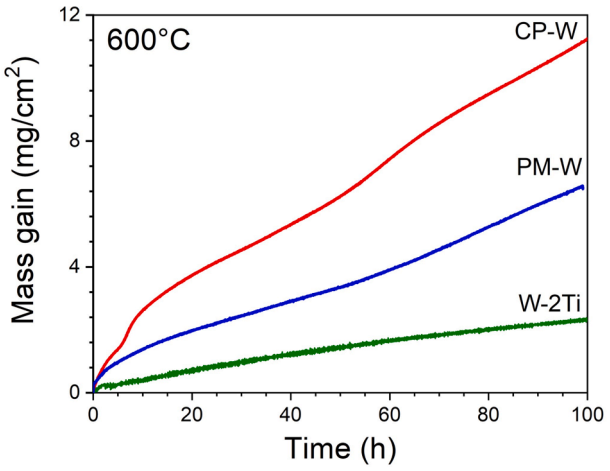

Fig. 11. Comparison among the isothermal mass gain curve for W-2Ti oxidized for 100 h at 600 °C with those of pure tungsten processed by two different routes; Conventional processing CP-W [8] and powder metallurgy PM-W [12].

the aspect of mass gain curves is completely different depending on the oxidation temperature.

The major increase in the mass gain of pure tungsten materials is related to short periods of time in which the parabolic growth of the scale changes to a linear one. Since the number of these accelerated growth events is higher for the CP-W than for PM-W, two and one

respectively, the highest mass gain corresponds to CP-W. Almost linear growth at 600 °C in pure tungsten is caused by local microcracking in the initially protective $W_{18}O_{49}$ layer. The considerable volume change associated with the oxidation of tungsten into any kind of tungsten oxide (the Pilling-Bedworth ratio for WO_3 is 3.3) induces high stresses which are released by localised microcracking in the scale [8,19], allowing oxygen to easily reach the surface of the alloy to form other less protective oxides such as $WO_{2.92}$. As the oxidation proceeds, the oxygen gradient through the scale continuously changes decreasing from the surface to the interior of the scale. $WO_{2.92}$ should transform progressively into WO_3 when oxygen partial pressure rises up to the level in which WO_3 could grow [8]. Since no microcracking was noticed in the scale during oxidation of W-2Ti alloy, the WO_3 scale cannot result from the progressive transformation of $W_{18}O_{49}$ into WO_3 through the formation of intermediate $WO_{2.92}$.

To verify this point, a W-2Ti sample was oxidized for 1 h and the oxides constituting the layer were identified by XRD measurements. The corresponding XRD pattern is presented in Fig. 12, showing that the oxide scale is mainly composed by $W_{24}O_{68}$ (also named $WO_{2.83}$) and $W_{18}O_{49}$ (also known as $WO_{2.72}$), while small peaks at 47.25° and 69° correspond to tungsten. This result differs from that reported for pure tungsten, in which the oxide layer developed in the first hour of exposure consists of $W_{18}O_{49}$ and $WO_{2.92}$ [8]. Since protective non-stoichiometric tungsten oxides, like $W_{18}O_{49}$ and $W_{24}O_{68}$, are found from the early stages of oxidation, the beneficial effect of small additions of titanium is not related to a change in the nature of the oxides composing the scale. It could arise from the fact that Ti could be oxidized internally as TiO_2 or a mixed W-Ti oxide. This agrees with results reported during short-term oxidation of W-10Ti (wt%) coatings where small TiO_2 particles grow at grain boundaries of the tungsten oxide layer, obstructing inward oxygen diffusion along grain boundaries [21,22].

In the case of the present W-2Ti alloy, Ti-containing oxides were probably not detected in XRD patterns because of their small size and low volume fraction, but EDX microanalyses reveals that the dark regions in the scale are slightly enriched in titanium. Consequently, it could be assumed that the main effect of such Ti-containing oxides would be to break the continuity of tungsten oxides in such a way that the typical columnar structure of oxide grains developed during the oxidation of pure tungsten [8,12] is replaced by other more equiaxed. This effect produced a dramatic difference between the W and W-2Ti oxidized samples that can be clearly observed with the naked eye. The tested 10 × 10 × 1 mm^3 coupons used for oxidation tests developed a Maltese cross-like aspect for the oxidized pure W sample due to the exacerbated growth of the oxide scale, as it is shown in the inset of Fig. 10 of Reference [8], which was absent in the W-2Ti oxidized samples. The equiaxed microstructure of the oxide scale minimizes the large growth stresses associated with tungsten oxides, minimizing the tendency for massive microcracking in the scale. Nevertheless, the protective nature of this scale is less to that provided by $W_{18}O_{49}$ in pure tungsten as can be clearly inferred from the slightly higher value of the oxidation rate exponent in the steady state: n = 0.75 alloy for W-2Ti and 0.65 and 0.5 for pure CP-W and PM-W materials, respectively. However, the beneficial effect of the absence of microcracking in the scale formed on the W-2Ti alloy balances the less protectiveness provided by the less dense scale so that the total mass gain is much lower in the case of the W-2Ti alloy than for pure CP-W. This behaviour could indicate that the interfaces observed at dark regions, where Ti-containing oxides are present, could act as rapid pathways for inward oxygen transport into the alloy, resulting in the slightly higher values of the oxidation rate exponent observed in the steady state. Other aspect contributing to the lower mass gain of W-2Ti alloy is that the time required to attain the steady state is much shorter for the W-2Ti alloy than for pure tungsten materials. As Fig. 11 evidences, the mass gain of CP-W and PM-W materials after 5 h of exposure is 5 and 3.5 times higher, respectively, than that of W-2Ti alloy. This demonstrates that the rapid accomplishment of the steady state is a critical factor to reduce the total mass gain of W-2Ti alloy and, therefore, the addition of titanium addition should shorten the period needed for establishing a protective $W_{18}O_{49}$ layer.

The decrease in mass gain is even more noticeable at 700 °C than that found at 600 °C, being the mass gain at least ten times lower (see Fig. 13) and the oxide scale eight times thinner than those reported for pure CP-W or PM-W [8,12]. The protective nature of the scale developed at this temperature is reflected in the decrease in the oxidation exponent

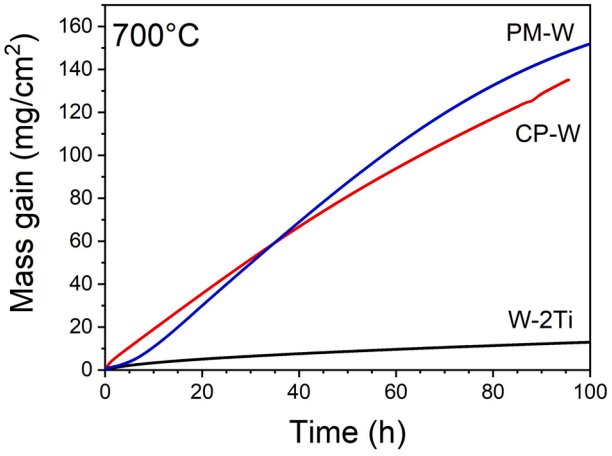

Fig. 13. Comparison among the isothermal mass gain curve for W-2Ti oxidized for 100 h at 700 °C with those of pure tungsten processed by two different routes; Conventional processing CP-W [8] and powder metallurgy PM-W [12].

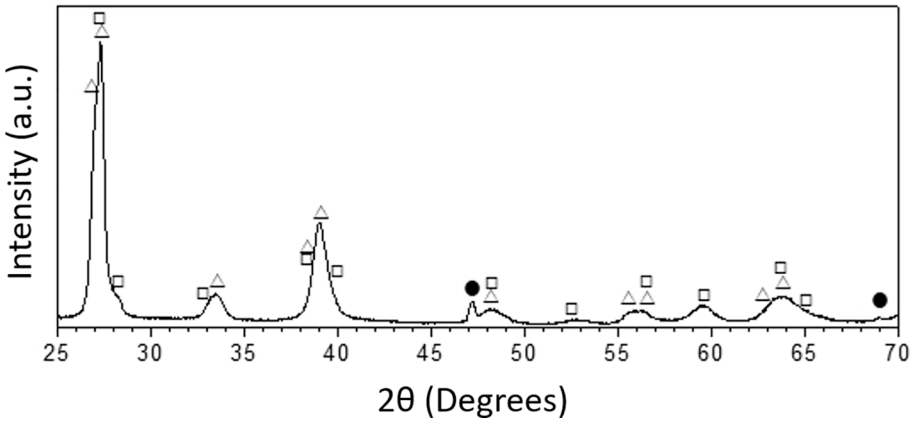

Fig. 12. XRD pattern of the oxide scale formed on W-2Ti alloy after oxidation at 600 °C for 1 h (•-W, □-$W_{19}O_{48}$, Δ-$W_{24}O_{68}$).

compared with the value calculated at 600 °C, 0.6 against 0.75, respectively. This probably is related to the densification of the innermost part of the scale during the inward growth of the oxide, so inward oxygen flow towards the oxide/alloy surface is reduced because of the decrease in the number of cavities/pores which could act as rapid-pathways for oxygen ingress. The structure of the scale is totally different to that reported during oxidation of pure tungsten which consists of a multilayered structure resulting from periodical massive events of cracking in the scale close to the scale/metal interface, so major effect of titanium addition is reducing growth stresses in the scale. EDX measurements in the grey coloured regions of the scale evidence certain titanium enrichment, suggesting that the formation of small particles of a Ti-containing oxide prevents the directional growth of tungsten oxides, minimizing in this way growth stresses within the scale. This suppression of cracking events within the oxide scale results in the excellent oxidation behaviour of the W-2Ti alloy.

At 800 °C, the improvement on the oxidation behaviour is even better compared to the behaviour of pure tungsten because the total mass gain of the W-2Ti alloy after 100 h of exposure is practically the half of pure CP-W or PM-W oxidized just for 20 h (see Fig. 14). The multilayered pattern of the tungsten scale developed on pure tungsten is absent in the W-2Ti alloy. Nevertheless, the oxidation mechanism experiences changes in the course of the oxidation exposure at this temperature. Kinetic curves evidence the occurrence of short periods of time where the scale loses suddenly its protective character (see Fig. 14), as can be deduced from the shifting of the stress exponent from values close to parabolic (n≈0.5) to values higher than linear (n < 1).

This can be clearly seen in the structure of the oxide scale as the oxidation progress. During the initial stages of oxidation, the scale is relatively uniform and dense and only Ti-pools appears interrupting the continuity of the scale. As the oxidation progresses, an abrupt increase in mass gain is observed at about 25 h, which is followed by a period at which the kinetics tend to obey parabolic kinetics. Observation of the sample exposed for 30 h, confirms the existence of a sharp discontinuity in the middle of the scale (see Fig. 9), showing on both sides of the discontinuity almost the same structure found after long-term oxidation at 700 °C. The observed sudden increase in the oxidation rate is caused by this massive fail in the scale due to the large continuous crack parallel to the scale. The subsequent decrease in mass gain indicates that the protective layer is re-established again until a new event of massive cracking takes place, as observed in the sample exposed for 100 h (see Fig. 10). At this time, a second large discontinuity/macrocrack is found within the scale, which coincides with the second breakdown of the parabolic behaviour in the mass gain curve.

5. Conclusions

Addition of 2 wt% titanium to tungsten results in a considerable improvement of the oxidation resistance of the alloy, increasing the temperature for the use of tungsten in the event of a LOVA accident to 700 °C in compliance with the top-level safety objectives for a nuclear fusion plant [23]. Even at 800 °C, the lifetime of W-2Ti alloy is significantly extended compared to pure tungsten. Compared to pure tungsten the mass gain of W-2Ti alloy is reduced five times at 600 °C, ten times at 700 °C and eight times at 800 °C. The beneficial effect of Ti addition is related to prevent directional growth of WO_3, so growth stresses in the scale are significantly reduced in such a way that massive cracking events, responsible of accelerated mass gain in tungsten, are suppressed at 600 and 700 °C, and significantly mitigated at 800 °C.

CRediT authorship contribution statement

P. Pérez: Conceptualization, Methodology, Validation, Formal analysis, Investigation, Writing – original draft, Writing – review & editing, Visualization, Supervision, Data curation. **M.A. Monge:** Resources, Conceptualization, Methodology, Validation, Formal analysis, Investigation, Writing – original draft, Writing – review & editing, Visualization, Supervision, Project administration, Funding acquisition.

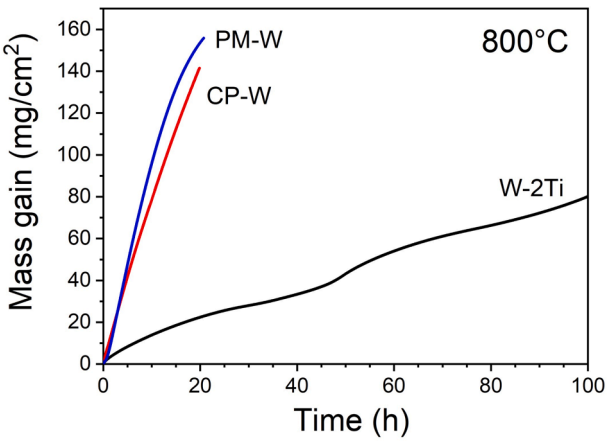

Fig. 14. Comparison among the isothermal mass gain curve for W-2Ti oxidized for 100 h at 800 °C with those of pure tungsten processed by two different routes; Conventional processing CP-W [8] and powder metallurgy PM-W [12].

Declaration of Competing Interest

The authors declare that they have no known competing financial interests or personal relationships that could have appeared to influence the work reported in this paper.

Acknowledgements

This research was supported by the Agencia Estatal de Investigación of Spain (PID2019-105325RB-C33/AEI/10.13039/501100011033) and by the Regional Government of Madrid through TECHNOFUSIÓN(III) CM (S2018/EMT-4437) project cofinanced by Structural Funds (ERDF and ESF). The support of the Regional Government of Madrid through the multi-annual agreement with UC3M (Excellence of University Professors–EPUC3M14 and in the context of the V PRICIT - Regional Programme of Research and Technological Innovation) is also acknowledge.

References

[1] D. Stork, S.J. Zinkle, Introduction to the special issue on the technical status of materials for a fusion reactor, Nucl. Fusion 57 (9) (2017) 092001.
[2] G. Mazzone et al., Eurofusion-DEMO Divertor - Cassette Design and Integration. Fusion Eng. Des. 157 (2020) 111656. DOI: j.fusengdes.2020.111656.
[3] J.W. Davis, V.R. Barabash, A. Makhankov, L. Plöchl, K.T. Slattery, Assessment of tungsten for use in the ITER plasma facing components, J. Nucl. Mater. 258–263 (P1) (1998) 258–263, https://doi.org/10.1016/s0022-3115(98)00285-2.
[4] A. Hasegawa, M. Fukuda, T. Tanno, S. Nogami, Neutron irradiation behavior of tungsten, Mater. Trans. 54 (4) (2013) 466–471, https://doi.org/10.2320/matertrans.MG201208.
[5] M.R. Gilbert, T. Eade, T. Rey, R. Vale, C. Bachmann, U. Fischer, N.P. Taylor, Waste implications from minor impurities in European DEMO materials, Nucl. Fusion 59 (7) (2019), 076015, https://doi.org/10.1088/1741-4326/ab154e.
[6] T. Hirai, et al., Status of technology R&D for the ITER tungsten divertor monoblock, J. Nucl. Mater. 463 (2015) 1248–1251, https://doi.org/10.1016/j.jnucmat.2014.12.027.
[7] S. Piet, E. Cheng, L. Porter, Accident safety comparison of elements to define low-activation materials, Fusion Technol. 17 (1990) 636–657, https://doi.org/10.13182/FST17-4-636.
[8] S.C. Cifuentes, M.A. Monge, P. Perez, On the oxidation mechanism of pure tungsten in the temperature range 600–800 °C, Corros. Sci. 57 (2012) 114–121, https://doi.org/10.1016/j.corsci.2011.12.027.
[9] A. Malizia, L. Poggi, J.-F. Ciparisse, R. Rossi, C. Bellecci, P. Gaudio, A review of dangerous dust in fusion reactors: from its creation to its resuspension in case of LOCA and LOVA, Energies 9 (8) (2016) 578.
[10] M.R. Gilbert, J.-C. Sublet, Neutron-induced transmutation effects in W and W-alloys in a fusion environment, Nucl. Fusion 51 (4) (2011) 043005.
[11] M.A. Monge, P. Adeva, A. Muñoz, P. Pérez, Oxidation behaviour of tungsten with vanadium additions, Fusion Eng. Des. 146 (2019) 783–786.

[12] S.C. Cifuentes, A. Muñoz, M.A. Monge, P. Pérez, Influence of processing route and yttria additions on the oxidation behavior of tungsten, J. Nucl. Mater. 442 (2013) S214–S218, https://doi.org/10.1016/j.jnucmat.2012.10.033.
[13] P. Pérez, M.A. Monge, A. Muñoz, P. Adeva, Influence of 1 and 5 wt% TiC additions on the oxidation behaviour of pure tungsten, Nucl. Mater. Energy 24 (2020), 100780, https://doi.org/10.1016/j.nme.2020.100780.
[14] M.V. Aguirre, A. Martín, J.Y. Pastor, J. LLorca, M.A. Monge, R. Pareja, Mechanical properties of Y2O3-doped W-Ti alloys, J. Nucl. Mater. 404 (3) (2010) 203–209.
[15] A. Muñoz, B. Savoini, E. Tejado, M.A. Monge, J.Y. Pastor, R. Pareja, Microstructural and mechanical characteristics of W–2Ti and W–1TiC processed by hot isostatic pressing, J. Nucl. Mater. 455 (2014) 306–310, https://doi.org/10.1016/j.jnucmat.2014.06.064.
[16] A. Muñoz, M.A. Monge, B. Savoini, R. Pareja, A. Radulescu, SANS characterization of particle dispersions in W-Ti and W-V alloys, Int. J. Refract. Metals Hard Mater. 61 (2016) 173–178, https://doi.org/10.1016/j.ijrmhm.2016.09.009.
[17] R.G. Palgrave, I.P. Parkin, Aerosol assisted chemical vapour deposition of photochromic tungsten oxide and doped tungsten oxide thin films, J. Mater. Chem. 14 (19) (2004) 2864.
[18] S. Bandi, A.K. Srivastav, Unveiling the crystallographic origin of mechanochemically induced monoclinic to triclinic phase transformation in WO_3, Cryst. Eng. Comm 23 (2021) 1821–1827, https://doi.org/10.1039/D0CE01813A.
[19] E.A. Gulbransen, K.F. Andrew, Kinetics of the oxidation of pure tungsten from 500 to 1300 °C, J. Electrochem. Soc. 107 (1960) 619–628, https://doi.org/10.1149/1.2427787.
[20] E.A. Gulbransen, K.F. Andrew, F.A. Brassart, Kinetics of oxidation of pure tungsten, J. Electrochem. Soc. 111 (1964) 103–109, https://doi.org/10.1149/1.2426043.
[21] C. Louro, A. Cavaleiro, Thermal oxidation of tungsten-based sputtered coatings, J. Electrochem. Soc. 144 (1) (1997) 259–266.
[22] A. Cavaleiro, C. Louro, F. Montemor, Oxidation of sputtered W-based coatings, Surf. Coat. Technol. 131 (2000) 441–447, https://doi.org/10.1016/S0257-8972(00)00784-2.
[23] International Atomic Energy Agency 1999 Basic Safety Principles for Nuclear Power Plants 75-INSAG-3 Rev. 1. Report by the International Nuclear Safety Advisory Group (INSAG-12), IAEA, Vienna (1999) (www-pub.iaea.org/MTCD/Publications/PDF/P082_scr.pdf).